Time-dependent influence of high glucose environment on the metabolism of neuronal immortalized cells

Laura Colombaioni[1], Beatrice Campanella[2,*], Riccardo Nieri[2], Massimo Onor[2], Edoardo Benedetti[3] and Emilia Bramanti[2]

[1] Consiglio Nazionale delle Ricerche, Istituto di Neuroscienze, via Giuseppe Moruzzi 1, 56124, Pisa, Italy; laura.colombaioni@in.cnr.it
[2] Consiglio Nazionale delle Ricerche, Istituto di Chimica dei Composti Organometallici, via Giuseppe Moruzzi 1, 56124, Pisa, Italy; riky.46@hotmail.it, massimo.onor@pi.iccom.cnr.it, emilia.bramanti@pi.iccom.cnr.it
[3] Unità di Ematologia, Dipartimento di Oncologia, Università di Pisa, via Roma 67, 56100, Pisa, Italy; edobenedetti@gmail.com
* Correspondence: beatrice.campanella@cnr.it; Tel.: +39 050 315 2964

Abstract: In this work the effect of glucose concentration on the metabolome of living hippocampal HN9.10e neurons was studied. This cell line represents a reliable, *in vitro* model of one of the most vulnerable regions of central nervous system. Targeted metabolites were analyzed in the cell culture medium by two direct methods, namely liquid chromatography – diode array detection and headspace – solid phase micro extraction – gas chromatography – mass spectrometry. Twenty-two metabolites were simultaneously identified and quantified in the growth medium of the cells, treated with 25, 50 or 75 mM glucose, sampled along 8 days to mimic a prolonged hyperglycemia. The results of statistical analysis showed the clear impairment of neuronal metabolism already after 48 hours, represented by a significant reduction of the metabolic activity.

Keywords: Targeted metabolomics; hyperglycemia; primary cultured hippocampal neurons; HPLC-DAD; cell death; 3-way PCA.

1. Introduction

Glucose is an energetic substrate essential for our brain, but its excess strongly affects brain metabolism giving serious pathological consequences.[1] Cerebral glucose metabolism is tightly linked to neuronal metabolism[2] likely because of the ATP-sensitive potassium (KATP) channels, which are found in many excitable cells, including cardiac myocytes, pancreatic β cells, and neurons.[3,4]

Cho et al. found that high glucose induced apoptosis in SH-SY5Y neuronal cells via the mitochondria-dependent pathway due to the mitochondria oxidative phosphorylation, cell death regulation, and ROS production.[5] Macauley et al. reported that high glucose levels typical of type 2 diabete alter both hippocampal interstitial fluid Aβ levels and neuronal activity in mice, acting as pharmacological manipulation of KATP channels in the hippocampus. KATP channel activation mediates the response of hippocampal neurons to hyperglycemia by coupling metabolism with neuronal activity.[6] Elevated extracellular glucose levels can evoke indeed rapid changes in neuronal excitability through KATP channel closure and, thus, membrane depolarization.[3]

Recent studies in primary cultured hippocampal neurons report that high glucose (from 50 up to 150 mM) for 24, 48, 72 and 96 h is the main factor of diabetic cognitive impairment and can cause hippocampus abnormalities due to ROS generation.[7] In their work Russell and co-workers indicate that 45 mM glucose levels induce reactive oxygen species (ROS) production, mitochondrial membrane depolarization, partial depletion of ATP, and activation of caspase-3 and -9 that precedes neuronal apoptosis.[8] Studies have demonstrated that hyperglycemia arising from diabetes induces peripheral sensory neuronal impairment and mitochondrial dysfunction.[9] Furthermore, there is evidence that the hippocampal dysfunction in diabetic animals might result in cognitive deficits and increases the risk of depression and dementia.[10]

It is known that in the central nervous system of many vertebrates, including humans, the neurogenesis continues during the adulthood. This process has been well documented in neocortex, in striatum[11,12] and, in particular, in hippocampus.[13] The hippocampal neurogenesis is required for learning and memory processes,[14,15] and it is also responsible of many different pathologies including mood disorders, stress and epilepsy.[16,17] Thus, the specific conditions able to influence the neurogenesis must be carefully addressed in the view that their deregulation could increase the risk of abnormalities in cognitive function.

Due to the role of hyperglycemia in neurodegenerative diseases[18], and to the severe damage of hippocampal region in this kind of pathologies[19], the study of the effects of glucose in proliferating neurons is of crucial importance. By contrast, these cells are still largely uncharacterized from a metabolic point of view and, in particular, the consequences of an elevated glucose exposure remain mostly unexplored. The effect of high-glucose environment on neuron metabolism was studied using nuclear magnetic resonance (NMR)-based metabolomics in primary neuron cultures to contribute to the understanding of the metabolic alterations and underlying pathogenesis of cognitive decline in diabetic patients.[20]

In this work we studied the effect of glucose concentration in living hippocampal HN9.10e neurons, a somatic fusion product of hippocampal cells from embryonic day 18 C57BL/6 mice and N18TG2 neuroblastoma cells.[21] This cell line shares many structural and functional features with primary hippocampal neurons and, consequently, it is a reliable *in vitro* model of one of the most vulnerable regions of central nervous system.[22] Since HN9.10e is a well-characterized cell line from the morphological and functional point of view, it allows a reliable evaluation of minute metabolic alterations, which is currently missing in the literature.

2. Results

2.1. Glucose influences the growth rate and viability of HN9.10e neuroblasts.

The effects of glucose on the neuronal growth were evaluated as confluence fraction of the cell population, whose values are reported in Fig 1A and in Supplementary Table 1S.

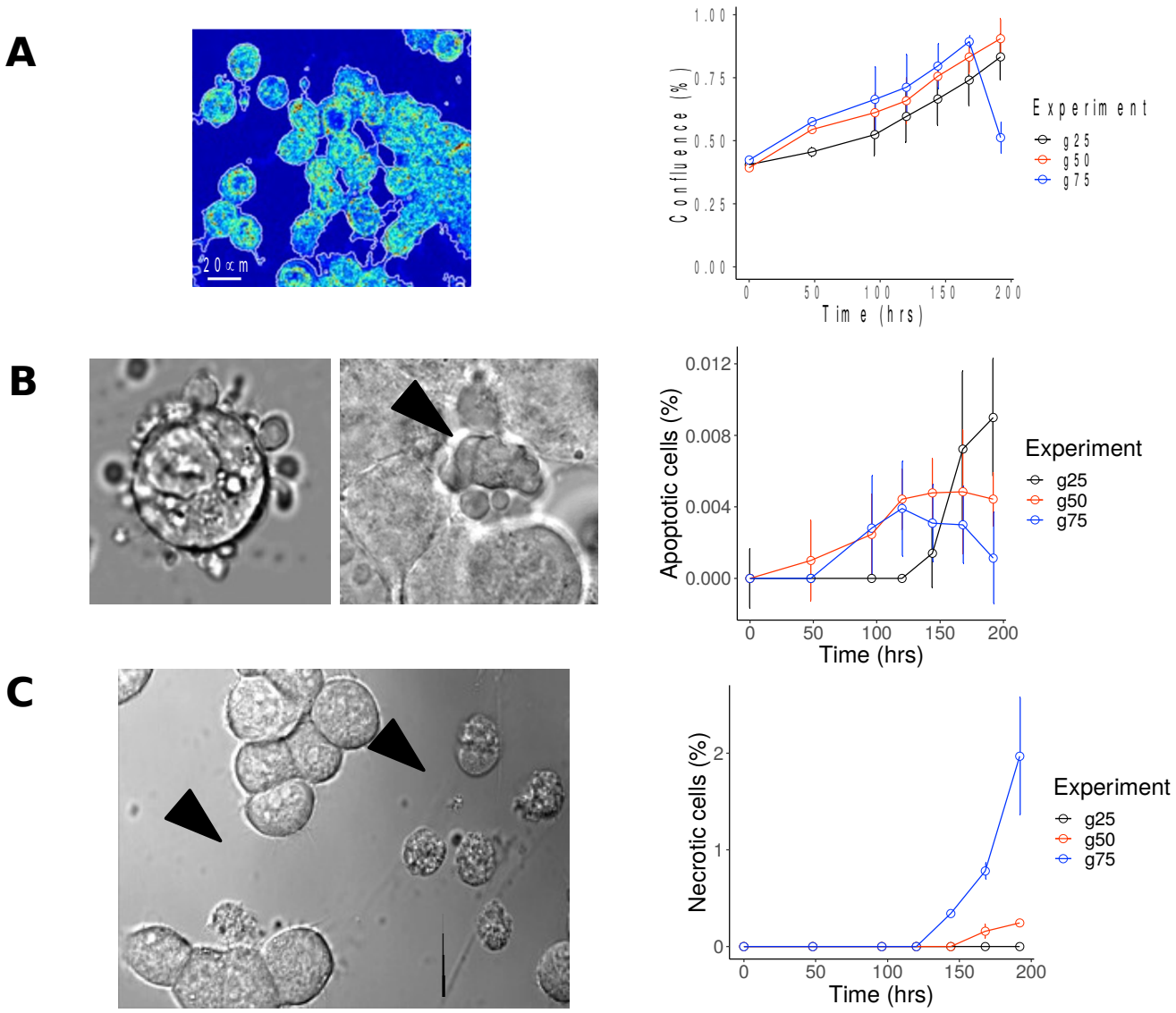

Figure 1. Effect of glucose on growth rate and viability. A) Left: a representative image illustrates the typical cell contouring by the Matlab scientific software. The ratio [surface occupied by cells/cell-free surface] is used to quantify cell density and growth rate in cultures incubated with 25, 50, 75 mM glucose. Right: the cell confluence fraction for the different glucose concentrations. Each value represents the mean of the ratio [surface occupied by cells/total surface] measured in n = 5 independent, non-overlapping fields 400 x400 µm (SD < 2%; p<0.01). **B)** Representative images of apoptotic HN9.10e neuroblasts in early (left) or late phase (middle), arrow indicates a typical collapsed and fragmented nucleus. Right: apoptosis incidence for the different glucose concentrations (SD<2%; p<0,001). **C)** Left: typical necrotic morphology: arrows point to HN9.10e neuroblasts dying for necrosis. Right: necrosis incidence for the different glucose concentrations (SD<2%; p<0,001). Apoptotic and necrotic cells were counted in the same fields in which confluence was quantified.

Cell confluency increased linearly with time up to 192 h. In hyperglycemic conditions (50 and 75 mM) a higher growth rate, compared to the basal condition (25 mM), is demonstrated by the slope of the confluence fraction curve, particularly during the first 96 h of treatment (T0-T2). Only in cultures treated with 75 mM glucose the cell confluence decreased abruptly and significantly at 192 h (T6).

Starting from 120 h (T3) the growth rate in glucose 50 and 75 mM decreased, probably due to an increase in the incidence of cell death. To clarify the impact of cell death, a specific analysis of the

apoptosis and necrosis incidence in the different experimental conditions was made. Apoptotic and necrotic cells were distinguished on the basis of their standard, well recognized, morphological features.[23] The early phase of apoptosis is characterized by blebbing of the plasma membrane without integrity loss, followed by cytoplasmic shrinkage, nuclear collapse and formation of pyknotic bodies of condensed chromatin **(**Fig. 1 B left and middle). Necrotic cells exhibit loss of membrane integrity and disaggregated appearance in transmitted light microscopy (Fig. 1C left).

The apoptosis incidence was very low in each experimental group (<0.01%) (Fig.1B, right). Indeed, a minimal apoptosis incidence is a physiological phenomenon, corresponding to the normal cellular turnover of the culture. During the first 6 days (T0-T4), the apoptosis incidence slightly increased in 50 and 75 mM glucose compared to the basal condition (25 mM). This indicates a double effect of hyperglycemia: by one hand it increased the rate of cell proliferation, on the other hand, it also increased the apoptosis incidence. This suggests an enhanced cellular vulnerability in high glucose conditions. However, it is evident that the neuronal energetics is still able to support the active process of apoptotic death during the first 6 days (T4) of culture.

In 25 mM glucose the apoptosis incidence linearly increased with the confluence and it typically reached the 0.01% value for a 95-98% confluence. On the contrary, a clear decrease of the apoptosis incidence was observed in high glucose starting from day 7 (T5): 0.005% in 50 mM, 0.003% in 75 mM compared to 0.007% in 25 mM glucose (4% relative standard deviation; $p<0.001$).

In parallel, the necrotic death, undetectable in any experimental group until day 5 (T3), increased considerably in 50 and 75 mM glucose beyond this time limit (Fig. 1C, right). The raise was gradual in 50 mM, but much more pronounced in 75 mM glucose, producing a sharp drop of the cell confluence value. The appearance of this massive necrosis suggests a severe energetic collapse, affecting more than 90% of the HN9.10e neuroblasts cultured in 75 mM glucose.

Based on these functional and morphological observations on living HN9.10e cultures, we did the exo-metabolites screening in CCM at corresponding times.

2.2. Metabolites quantified in HN9.10e culture medium.

SPME-HS-GC-MS and HPLC-DAD methods were here applied for targeted metabolomic analysis. On the basis of our previous works,[24,25] ethanol was selected among various volatile metabolites and monitored through SPME-HS-GC-MS. Twenty-one metabolites were found by HPLC-DAD in the samples analyzed, mainly belonging to glycolysis/gluconeogenesis, citrate cycle (TCA cycle), synthesis and degradation of ketone bodies, pyruvate metabolism and aminoacyl tRNA biosynthesis. The complete list of the quantified compounds, along with the respective concentrations, is presented in Supplementary Table 2S, along with their Human Metabolome Database (HMDB) ID and retention time.

2.3. Principal components analysis (PCA).

For statistical comparison, samples were divided in two sub-groups (i.e. basal at T0, all grown in 25 mM glucose, versus CCM samples at 48 h, and CCM sampled from 48 h to 168 h). The sampling point at 192 h (T6) was excluded from the analysis as the drop of cell confluency values suggests the massive release of metabolites due to cell necrosis.

First, samples at T0 (gx_T0, see Table 1S) and at T1 = 48 h (gx_T1, see Table 1S) were compared. All gx_T0 samples grown in 25 mM glucose and represent the reference basal condition, while gx_T1 (x = 25, 50 or 75) samples had experienced equal or increasing glucose

quantities. Principal component analysis was then performed, and it showed a good separation along Dim1 (which accounts for 76.5% of total variance) between cells grown in 25 mM glucose respect to those treated with 50 mM and 75 mM glucose (Figure 2). The second dimension differentiated samples treated with 50 mM glucose from those treated with 75 mM glucose, while cells grown in 25 mM glucose and collected after 48 h (g25_T1) clusterized with the respective basal (g25_T0). The analysis of loading plot (Figure 3) showed that the three basal samples and glc25_T1 are strongly positively correlated with all the metabolites, except oxidized nicotinamide adenine dinucleotide (NAD^+) (which is responsible for the separation of g50_T1), butyric acid and ethanol (both correlated with g75_T1).

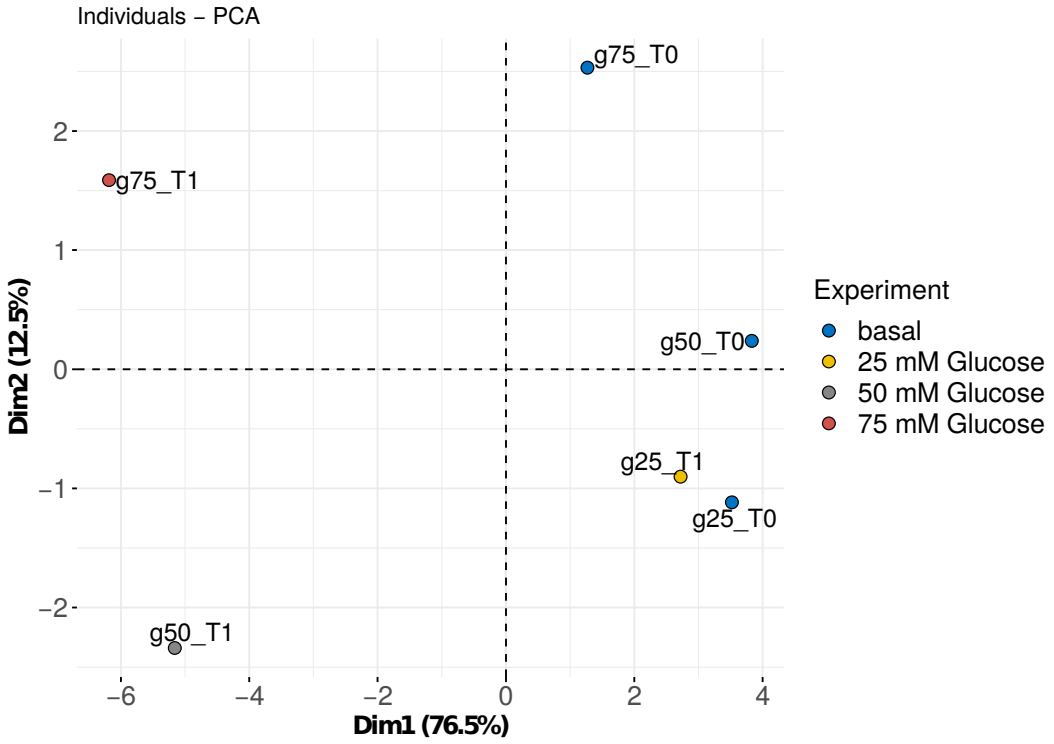

Figure 2. Principal component 1 (Dim1) versus principal component 2 (Dim2) score plot based on the result of principal component analysis. Percentage in the axis indicates the fraction of variance explained by the principal component.

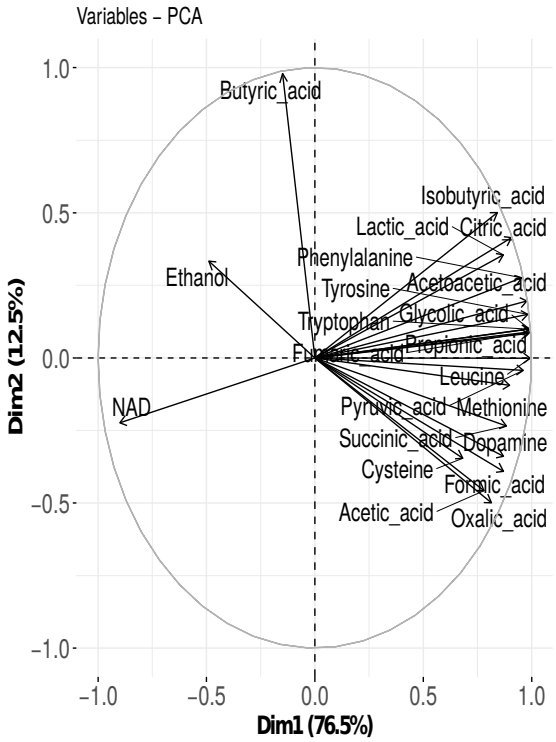

Figure 3. Principal component 1 (Dim1) versus principal component 2 (Dim2) loading plot based on the result of principal component analysis for samples gx_T0 and gx_T1 (x = 25, 50 or 75 mM glucose).

PCA was also used to represents samples from gx_T1 to gx_T5 (x = 25, 50 or 75), representing the temporal evolution of the three classes of experiments at increasing glucose concentrations. Figure 4 shows a clear separation through the second dimension of all g75 samples with respect to the others, while a weaker distinction appears along the first PC for g25 and g50 samples. Rather, the latter seems more influenced by the temporal evolution, with the samples moving from right to left with increasing time, i.e. the permanence of cells in the corresponding medium. The loading plot (Figure 5) mostly reflects the same plot obtained in the previous PCA. Here, the metabolites belonging to the TCA cycle (succinic acid, fumaric acid, propionic acid and citrate) are positively correlated among them and with the samples at 25 mM glucose analyzed after 48 (T1) and 96 h (T2), on the right side of score plot. With respect to the results of the PCA reported in figure 2 and 3, here ethanol is strongly correlated with NAD^+ and with the samples treated with 50 mM glucose. The hypothesis emerging from this analysis is that a high glucose concentration (i.e. 75 mM) induces a switching of HN9.10e neurons metabolism toward alternative metabolic pathways involving, in the case investigated, the production of butyric acid. At lower glucose concentrations (i.e. 50 mM) an alteration of metabolic pathways typical of normo-glycemic conditions likely occurs.

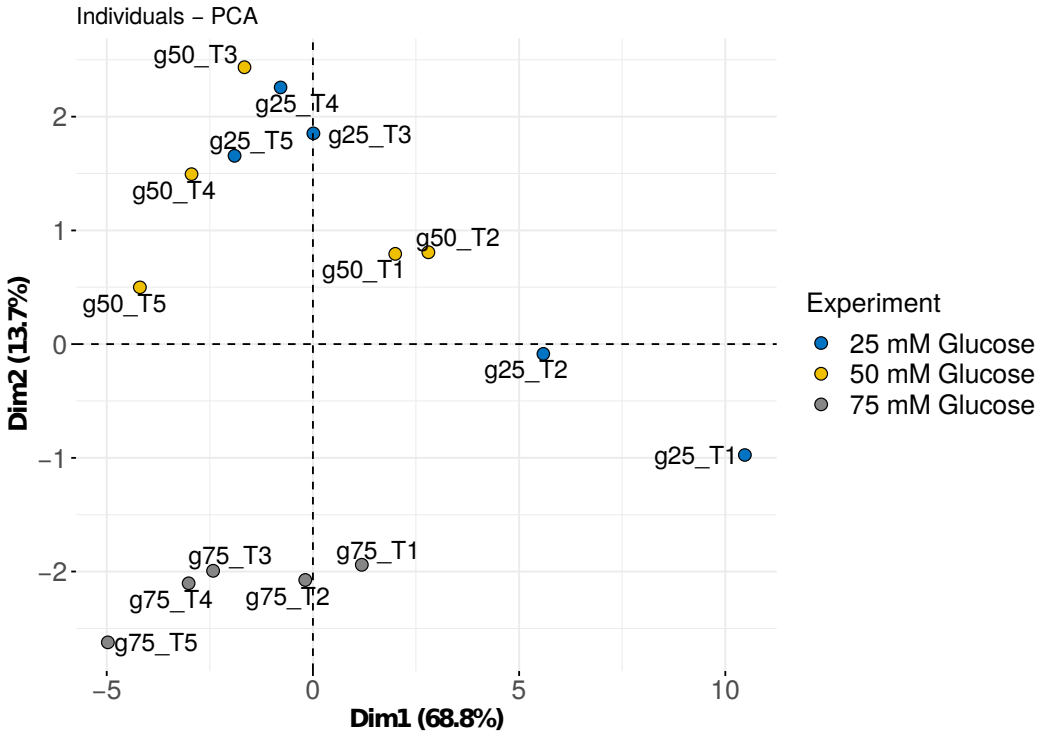

Figure 4. Principal component 1 (Dim1) versus principal component 2 (Dim2) score plot based on the result of principal component analysis. Percentage in the axis indicates the fraction of variance explained by the principal component.

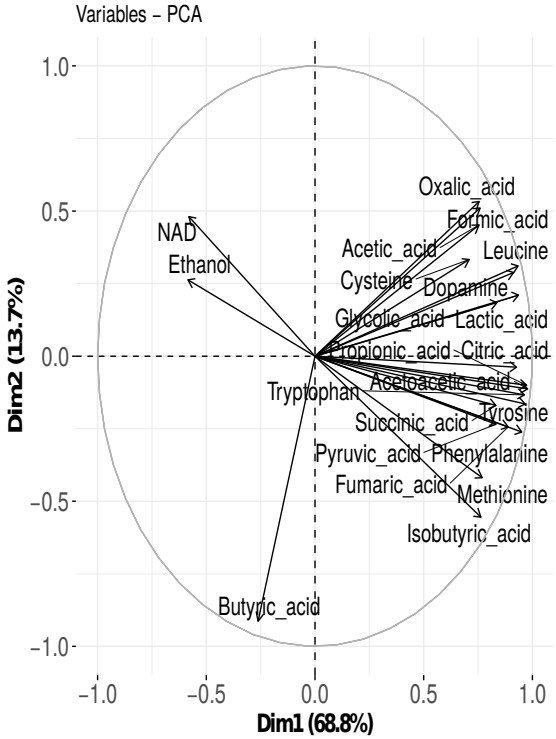

Figure 5. Principal component 1 (Dim1) versus principal component 2 (Dim2) loading plot based on the result of principal component analysis for samples from gx_T1 to gx_T5 (x = 25, 50 or 75 mM glucose).

2.4. Three-way Principal Component Analysis (3- way PCA).

PCA is generally not recommended to handle time-course data, which are non-independent. Here, PCA was used to have an overview of the quality of the acquired data. To further distinguish the

exact contribution of each variable to the observed changes in T1-T5 samples, 3-way PCA by applying the Tucker 3 model was performed to decompose metabolomic variations derived from time and glucose treatment.

3-way PCA is indeed particularly suitable for the management of three-dimensional data, especially when samples are analyzed over time. For a more complete treatment of this subject the reader should refer to [26].

The final results of 3-way PCA are three sets of loadings, which from a graphical point of view closely follow the score plot of standard PCA and whose relationship is described by a core array. Here, since two components for each mode (i.e. samples, variables and times, with I = 3, J = 22, K = 5) were retained, the final array is a cube having dimension [2,2,2]. The total variance of the *j*-scaled data explained by the Tucker model is 69.4%, which is fully satisfying considering the variability of a biological system. After body diagonalization, the following core array is obtained:

$$\begin{bmatrix} g_{111} & g_{121} & g_{112}\, g_{122} \\ g_{211} & g_{221} & g_{212}\, g_{222} \end{bmatrix}$$

$$\begin{bmatrix} 15.542 & 2.1486 & -0.21391 & -1.9009 \\ 0.76987 & 0.31494 & -5.1932 & -6.5705 \end{bmatrix}$$

Despite the matrix does not show a super-diagonal structure, the element $g_{1,1,1}$ is by far the largest one, followed by the element $g_{2,2,2}$. This behavior permits to display the three loading plots in a single triplot for the joint interpretation of the first two components for each mode.

From the plot of conditions (Figure 6), it can be noted that the data are elongated on Axis 1 and that the distance between the five points is not equal, similarly to the score plot of PCA. Three clusters can be identified as T1, T2 and T3-T4-T5. A possible interpretation is that the kinetics of the metabolic changes due to glucose treatment is not constant for each time lapse.

The points related to glucose treatment are spread along Axis 2, with the conditions at higher glucose concentration (50 and 75 mM) more closely related between them respect to the control at 25 mM. It has to be noticed that the 3-way PCA could detect the glucose effect much more efficiently than standard PCA.

Most of the variables are not influenced neither by time along Axis 1 nor by glucose concentration along Axis 2, with the exception of butyric acid and L-cysteine which appear oppositely correlated along Axis 2, and NAD^+ and ethanol, whose loadings are higher for Axis 1, i.e. they became significant for longer treatments (T3-T5) with 50 mM glucose.

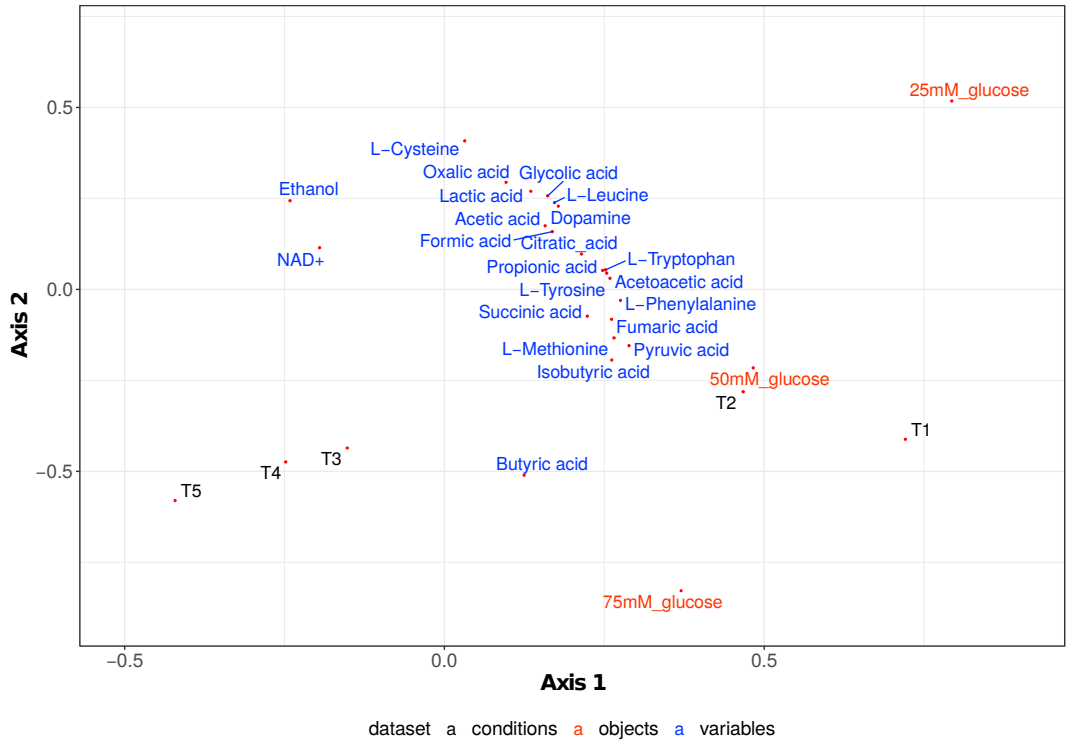

Figure 6. Results of 3-way PCA applied to the T1-T5 dataset.

Figure 7 reports the time dependent plots of NAD^+, butyric acid, L-cysteine and ethanol together with the trend of the metabolites belonging to the Kreb's cycle (succinic, fumaric, pyruvic and citric acid), while Figure S1 shows the rates of some key metabolites accumulation per 24h/normalized confluency.

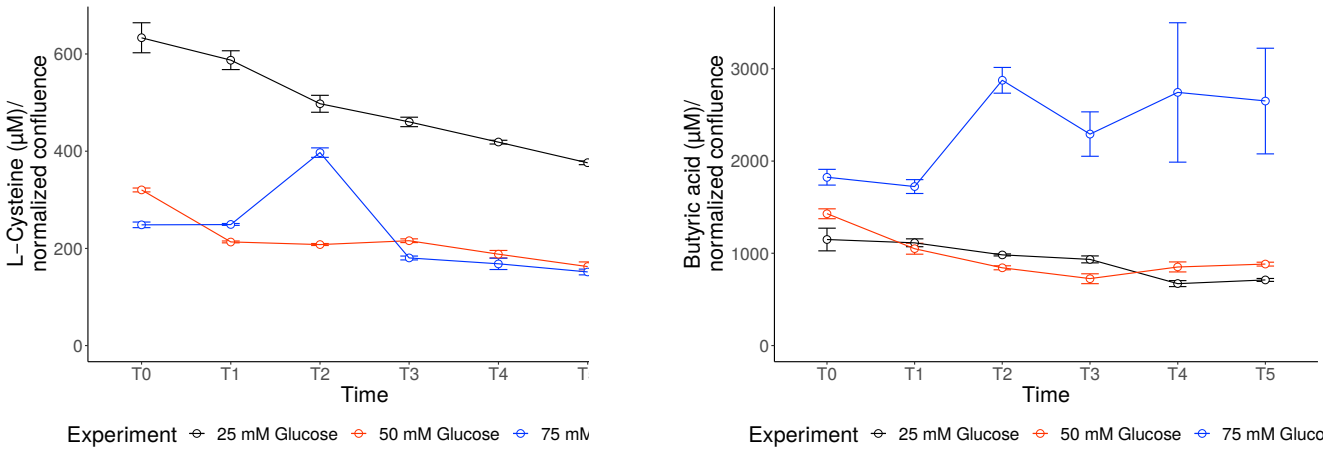

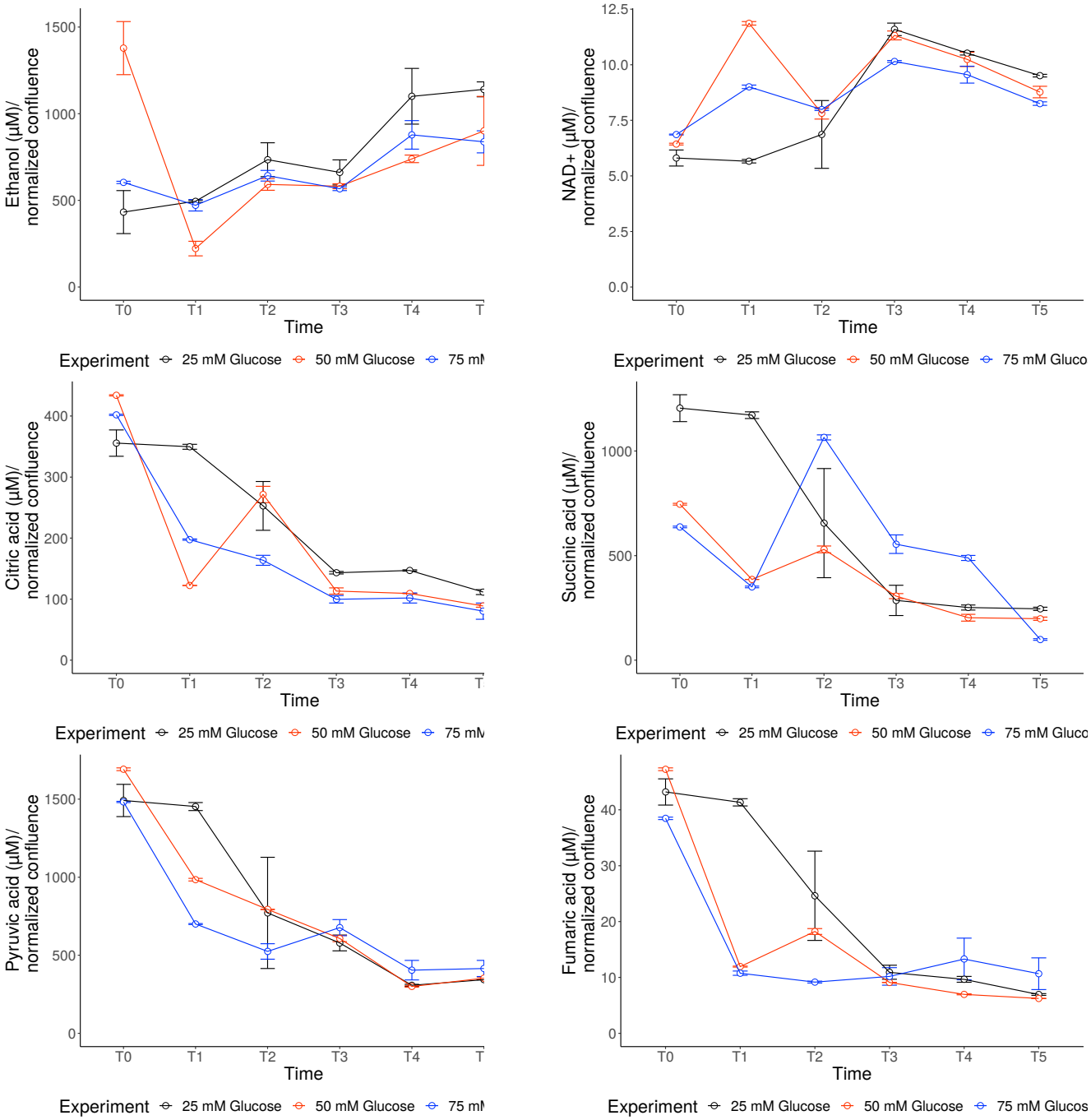

Figure 7. Trend of some key metabolites (i.e. L-Cysteine, butyric acid, ethanol and NAD^+ emerging from statistical analysis, and the metabolites from the Kreb's cycle) for each experimental condition (g25, g50 and g75). Error bars denote standard error of mean (SE).

3. Discussion

The effects of a high glucose environment on metabolome have been previously reported for cell lines from pancreas (BRIN-BD11 and INS-1E),[27] liver (HepG2)[28] and kidneys (HK-2).[29–31] In the studies mentioned, 25 mM was the maximum concentration of glucose employed to treat the cells, respect to a physiological glucose concentration equal to 5.5 mM.[32]

Due to the serious neurological complications associated with pathologies as diabetes, we propose here the HN9.10e hippocampal neuroblasts as model line to study hyperglycemia metabolic effects. The experimental conditions here adopted do not allow HN9.10e neuroblast differentiation since, due to the frequent change of CCM, the endogenously produced neurotrophins and growth factors cannot reach the optimal concentration required to trigger the differentiation process. Hence the cultures, remaining undifferentiated, represent a reliable *in vitro* model of proliferating hippocampal neuroblasts. The choice of examining the exo-metabolome instead of cell lysates is due to the relative simplicity of measuring over time and in the same cultured cells the variations of chemical composition in CCM, which rapidly provides the response of cells to external stimuli with a minimal perturbation of cell system.

Adherent neuronal cells are usually grown in the Dulbecco's Modified Eagle Medium (DMEM) containing 25 mM glucose, which here and in most of the studies dealing with neuroblasts represents a consolidated basal condition, because of the high metabolic rates of neuroblasts.[33] In a previous work, Liu et al. reported that the exposure of hippocampal neurons to 50 mM glucose was enough to provoke evident damages to cells. [7] They verified that the osmolality of glucose solutions between 25 and 150 mM being between 260 and 320 mOsm/kg, did not exert any effect on cell normal metabolism.[7]

In this work in addition to the basal concentration of 25 mM glucose we investigated the effects of 50 mM and 75 mM glucose, to verify the occurrence of a cellular metabolic shift.

We found that the cell viability in HN9.10e cells exposed to 75 mM glucose decreased remarkably after 8 days, compared to basal group, in line with previous studies and with the observation that long-term exposure to high glucose concentrations could impair the mitochondrial function inducing the hippocampal neurons dysfunction.[7] The sharp drop of cell viability of g75_T6 group is due to a massive necrosis process, as shown by the analysis with differential interference contrast microscopy. Other forms of cell death cannot be excluded, such as necroptosis, a regulated and active form of necrosis, typically triggered by inflammation and consistent with the enhanced ROS production induced by hyperglycemia.[34–36]

The metabolic impairment in HN9.10e embryonic hippocampal cells due to increasing glucose concentrations was studied by extracellular metabolites quantification. Although the panel of metabolites in our study was smaller if compared to untargeted mass spectrometry studies, this work was focused on several final products of cellular metabolism, which are known to represent the response of the cell to external stress.

Multivariate analysis and detailed metabolite level measurement show that the treatment with high doses of glucose induced a decrease of the concentration of metabolites from TCA cycle, which despite being intracellular intermediates here were found in the CCM. A reasonable hypothesis is the release of these metabolites in the extra-cellular medium by means of the monocarboxylate (MCTs), di- and tri-carboxylate transporters.[37,38]

The results obtained from 3-way PCA, which is a statistical technique suitable for the analysis of time-series, confirmed that neuronal cells have dose-dependent characteristic metabolic phenomena. Higher doses of glucose (75 mM in the case investigated) trigger in HN9.10e hippocampal neuroblasts deep metabolic alterations suggestive of the activation of "unconventional" metabolic pathways. These results are in agreement with the those found in HK-2 cell treated with various glucose concentrations by Wei et al. [31], where the increase of glycolysis and glucose oxidation was correlated to characteristic metabolic changes including increase in lactate-to-pyruvate ratio and suppression of TCA cycle.

HN9.10e hippocampal neuroblasts exposed to moderately high glucose levels (e.g. 50 mM in this cell system) ethanol production is strongly stimulated respect to basal condition, and NAD^+ levels increase, but the increase of these metabolites seems more related to exposure time rather than to glucose level in CCM. The delay in the ethanol production agrees with a previous observation[25] and it could be related to an ancestral "safety procedure" which allows the cells to proliferate also when lactate concentration increases because mitochondrial function is effectively or apparently compromised or in hypoxic environments.[39]

The increase of adenine dinucleotide (NAD^+) is consistent with the reliance of neurons on glucose as an energy source, and it is subsequent to the conversion of excess pyruvate into lactate and ethanol, not regenerated because of the suppression of TCA cycle. The conversion of pyruvate regenerates NAD^+ and guarantees the support of the glycolytic flux.[39] It is well known, indeed, that the activity of lactate dehydrogenase is high in neurons.[40]

It is known that NAD^+ is an important energy substrate and cofactor involved in multiple metabolic reactions and that NAD^+ level is a critical determinant of neuronal survival.[41–44] It is also reported that NAD^+ attenuates excitotoxic death and preserved cellular NAD^+ levels to support sirtuin 1 and polymerase 1 activities, Ca^{++} homeostasis and, thus, it effectively coordinates mitochondrial function, metabolism and ageing.[41,45]

In brain NAD(H) de novo synthesis may occur only from niacin (vitamin B_3).[46] Liu et al. found that NAD^+ level affects the principle mechanism for neuronal survival during excitotoxic and ischemic conditions.[41] Neurodegenerative disorders characterized by protein accumulation, misfolding and proteotoxic stress have also been linked to NAD^+ depletion.[45]An increase of glycolysis enhances NADH oxidation to NAD^+, inducing an adaptive shift in energy metabolism. [47] Thus, it cannot be excluded that the increase of NAD^+ level has a signalling role to activate a salvage pathway in neurons. The impaired mitochondrial function, which is associated to many of these disorders, is, indeed, successfully restored by elevate cellular NAD^+ levels. It is known, indeed, the role of the rise of NAD^+ and sirtuin-activating compounds,[45,48] as well as the role of NAD^+ supplementation to reverse the impaired cell-energy metabolism and possibly oxidative stress that are implicated in AD cognitive decline,[44] and in aging and age-related diseases. [42,43]

The most intriguing result obtained in this work is the detection of high levels of butyric acid (BA), which was the main metabolite increasing after treatment with 50 and 75 mM glucose (see Figure 7). Butyrate is produced by several fermentation processes of obligate anaerobic bacteria starting from the glycolytic cleavage of glucose to two molecules of pyruvate. Three molecules of ATP are produced for each glucose molecule, a relatively high yield. Other pathways to butyrate include succinate reduction and crotonate disproportionation.

It is universally accepted that mammalian cells do not produce significant amounts of butyrate, and in humans the only significant sources are the microbiota and ingestion of dairy products. It is known, as well, that neurons are very sensitive to BA and its derivates (e.g. gamma-amino butyric acid, GABA or drugs). Cueno et al. reported that mM concentrations of BA induce oxidative stress, altered calcium homeostasis and neurite retraction in PC12 cells.[49] Cayo et al. showed that BA treatment of nerve growth factor (NGF)-untreated PC12 cells affected cell viability and lead to apoptosis induction.[50] Compounds derived from BA are gamma-amino butyric acid (GABA) and inhibitors of histone deacetylases (HDACs, butyric acid itself, valproic acid and 4-phenylbutyric acid).[51,52] Sharma et al. reported that 4-phenyl butyric acid (4-PBA) inhibits hyperglycemia-induced apoptosis in the dorsal root ganglion neuron.[51]

Nankova et al. reported that BA can regulate tyrosine hydroxylase (TH) mRNA levels in a PC12 cell model,[53] and that short chain fatty acids (SCFA) like propionic acid and BA produced by gastrointestinal bacteria are involved in the development of neuronal disorders including autism spectrum disorders influencing brain monoaminergic pathways (gut-brain axis).[54] All these results refer to the effects of exogenous butyric acid, i.e. BA administered to cell cultures or produced by intestinal bacteria.

The increase of BA found in this work is related to the endogenous production of BA by HN9.10e neurons metabolism. Currently, we have no proven explanations on the mechanism or mechanisms that were involved in the production of BA by primary hippocampal neurons. This issue requires further investigation.

It is known that glucose, once trapped in cells as glucose-6-phosphate, may go through glycolysis, pentose phosphate pathway or it can be employed for the glycogen synthesis.[55] However, neurons are not able to synthesize glycogen and their capacity to upregulate glycolysis is limited due to the constant proteasomal degradation in neurons of the enzyme 6-phosphofructo-2-kinase/fructose-2,6-bisphosphatase 3 (Pfkfb3), a key positive modulator of glycolysis in cells.[56,57] Thus, glucose is trapped in neurons as glucose-6-phosphate and it is mainly processed through the oxidative branch of the pentose phosphate pathway in neurons, rather than through glycolysis. This pathway is the main producer of reducing equivalents in the form of NADPH. In normoglycemic conditions NADPH is used to regenerate reduced glutathione, which is the main ROS scavenging agent in neurons and in less extent to synthesize fatty acids.

In the early stage of hyperglycemic conditions glycolysis and TCA is pushed by excess substrate, and neurons undergo oxidative stress with a high production of ROS. [7] Later, this likely induce a “metabolic reprogramming” in a “Warburg-like” phenotype, a TCA cycle suppression.[58] Thus, in hyperglycemia it is likely to suppose that neurons have a metabolic switch from oxidative phosphorylation toward non-oxidative glycolysis in the presence of oxygen, using glucose both in glycolysis for bioenergetic purposes cumulating pyruvate, lactate and ethanol, and redirect glucose as glucose-6-phosphate through the pentose phosphate pathway as “safety procedure” to increase NADPH production. The linear decrease of pyruvate concentration over the time at the three glucose doses (see Figure 7), confirms the metabolic switch. This metabolic reprogramming is found in several diseases related to oxidative stress, likely triggered by mitochondrial dysfunction and massive ROS production.[58]

The excess of glucose-6-phosphate and the consequent high consumption of NADPH in the first steps might avoid the elongation of short fatty acids. The hypothetical inhibition of the elongation steps could bring to butyric acid release from butyryl-ACP by a thioesterase enzyme.

Butyric acid is well known to modulate gene expression in elevated levels due to its action as a histone deacetylase,[59,60] and it is responsible for neuronal damage observed in short-chain acyl-CoA dehydrogenase deficiency (SCADD).[58] Accumulated butyric acid may be responsible for protein misfolding that causes oxidative damage, which is in a manner of a vicious circle with mitochondrial dysfunction. Its neurotoxicity may be responsible for the massive cell death observed at 192 h.

Considering the mitochondrion’s origin, i.e. the bacteria,[61] it can be hypothesized that any response of cell to stress agents that involve an alteration of energetic metabolism (high glucose concentration in this study, thallium contamination investigated in previous ones[24,25]) recalls ancestor mechanism to preserve cell vitality.

Figure 8 shows potential pathways that involve the metabolites determined in in HN9.10e cell lines and that significantly increase or decrease their extracellular concentration, assuming specific or aspecific transport outside the cells. For each metabolite the time evolution of the ratio of concentration level in 50mM glucose/25 mM glucose (red lines) and 75 mM glucose/25 mM glucose (black line) is shown. Figure 7 shows the enlargement of the time dependent plots of some key metabolites for an easier inspection. Direct data presenting the rates/time evolution of key metabolites accumulation per 24h/normalized confluency are also reported in Figure S1. The final *plateau* in the plots of metabolite variation (i.e. the difference in concentration between the sampling time Tx and T(x-1)) could be due to a reduced metabolic activity of the cells and/or to a depletion of TCA intermediates. In our experiment the CCM was refreshed at each sampling time point, thus the measurement of metabolites variation is an indication of the activity and vitality of the cell for each specific time window.

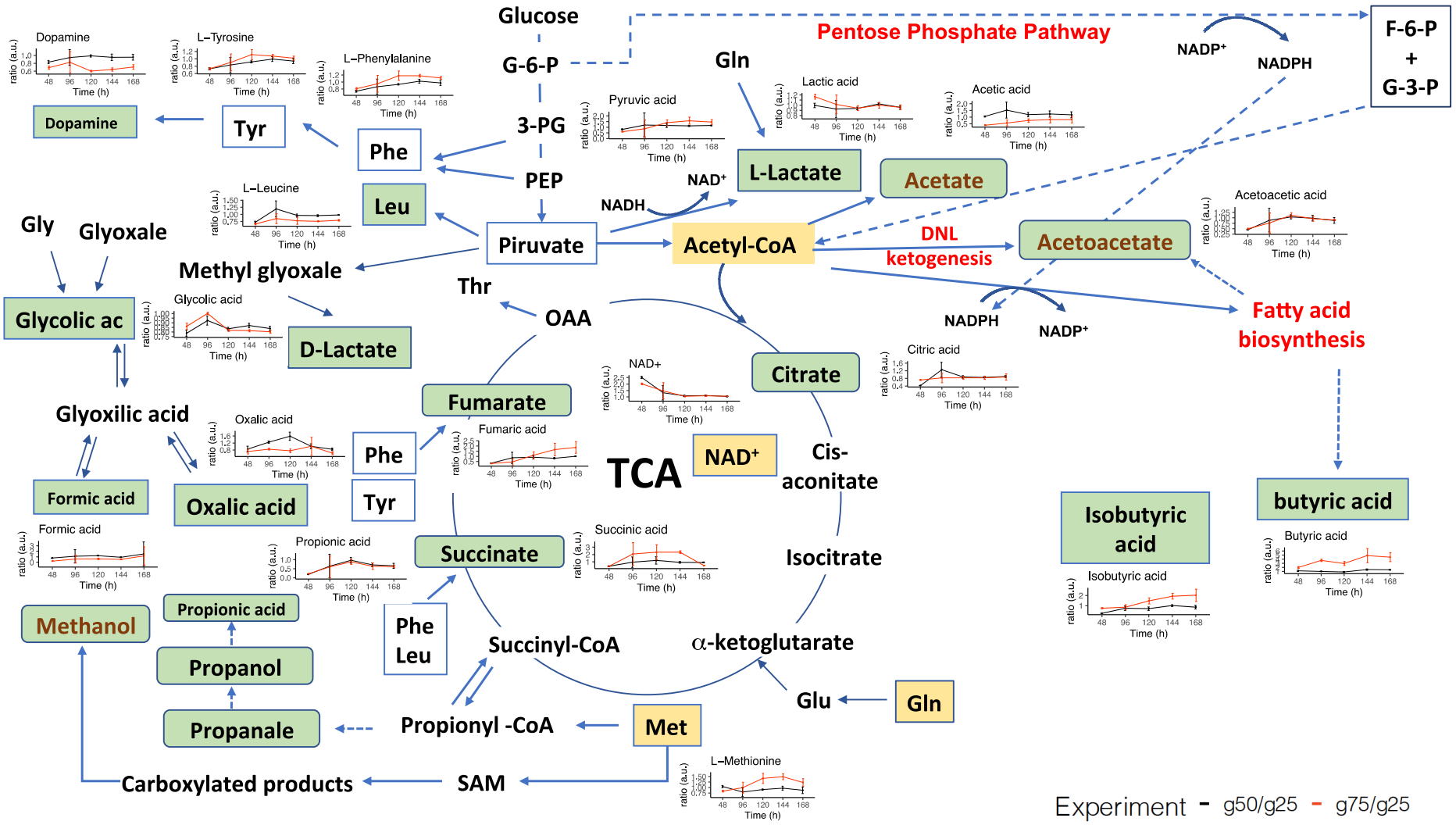

Figure 8. Potential pathways involving the metabolites determined in CCM of HN9.10e cell lines, assuming specific or aspecific transport outside the cells. Time resolved extracellular metabolite concentration in HN9.10e cell lines are reported as ratio for black: 50mM glucose / 25 mM glucose, red: 75 mM glucose / 25 mM glucose. Error bars denote standard error of mean (SE).

4. Materials and Methods

4.1. Chemicals.

Sulfuric acid for HPLC analysis was employed (30743 Honeywell Fluka 95-97%). Methanol for RP-HPLC was purchased from Merck (34860, ≥99.9%). Preparation/dilution of samples and solutions was performed gravimetrically using ultrapure water (MilliQ; 18.2 MΩ cm^{-1} at 25 °C, Millipore, Bedford, MA, USA).

Standard solutions for HPLC (TraceCERT®, 1000 mg/L in water) and ethanol (analytical standard for GC) were purchased from Sigma Aldrich (Milan, Italy). All compounds had purity higher than 98% and, thus, were used without any further purification. Analytes stock solutions were prepared by dissolving a weighed amount of the pure compound in deionized water and stored at 4°C up to 1 month.

All compounds had purity higher than 99% and thus were used without any further purification.

Solid Phase Micro-Extraction Fiber based on 85 um carboxen/polydimethylsiloxane (CAR/PDMS) were employed for the preconcentration of volatile compounds in the HS.

All chemicals, having purity higher than 99%, were purchased from Sigma-Aldrich (Italy) and used without any further purification. Working solutions were prepared by diluting standard stock solutions with milli-Q water and then stored at 4 °C up to 1 month in an amber vial until their use.

Helium 5.6 IP was purchased from Sol Group Spa (Italy) and was further purified with a super clean filter purchased from Agilent Technologies (USA) to remove water, oxygen and hydrocarbon contaminants. Solid-phase microextraction fiber based on 85 μm carboxen/polydimethylsiloxane was employed for the preconcentration of ethanol in the HS.

Preparation/dilution of samples and solutions was performed gravimetrically using ultrapure water (MilliQ; 18.2 MΩ cm^{-1} at 25 °C, Millipore, Bedford, MA, USA).

4.2. Cell culture and automated imaging of HN9.10e neuroblasts.

The experimental design adopted in this study is shown in Supplementary Table S1. To investigate the effects of high glucose culture medium, the HN9.10e hippocampal neuroblasts were incubated with three different doses of glucose representing a 2 and 3-fold increase from baseline (25 mM glucose). After 48 h of culturing in the basal condition (glucose 25 mM), glucose was kept 25 mM in CCM of control cultures and increased to 50 and 75 mM. Two independent batches for each glucose level were cultured. Cell culture medium (CCM) containing the established glucose concentration was collected and refreshed after the first 48h and successively every 24 h up to 192 h (8 days) after the beginning of the experiment.

The morphological and functional responses of HN9.10e neuroblasts to glucose increase in CCM were followed by differential interference contrast microscopy (also known as Nomarski interference contrast). This allowed enhancing the contrast of unstained neurons in the living cultures, avoiding the use of cell dyes or fluorescent probes. Indeed, the neuronal staining would imply a long permanence of dyes in CCM, due to the extended sampling and monitoring time (192 h). However, this could induce unpredictable metabolic alterations, or even a certain degree of vitality loss.

HN9.10e cells were grown in DMEM-F12 (1:1) medium HEPES buffered, supplemented with 4 mM L-glutamine, 50 UI/mL penicillin and 50 mg/mL streptomycin, at 37 °C in humidified atmosphere containing 5% CO_2. Cells, seeded at 20,000 cell/cm^2 in culture flasks containing 5 mL of medium, were left in culture for 4 days before treatments in order to allow substrate adhesion

and growth to an optimal 40 % confluence. After this, they were incubated in CCM containing 25, 50 or 75 mM glucose. To take account of variations, two independent batches of cells were cultured for each glucose level.

In order to analyze the cell morphology and growth rate avoiding the metabolic alterations or the viability loss potentially induced by the use of cell dyes, an inverted microscope (Axiovert 35, Carl Zeiss, Oberkochen, Germany) equipped with Nomarski interference contrast optics and 40x or 63x objectives was used. This set up allowed to monitor the growth and death events in unstained living cultures, without the need for any dye or fluorescent probe.

The degree of cell confluence was evaluated by the automated measure of the ratio [surface occupied by cells / cell-free surface] obtained after the cell boundaries were determined with the standard function "Edge Detection" of the MATLAB scientific software (The MathWorks, Massachusetts, U.S.A.), adapted to the specific contrast level and cell shapes of HN9.10e cultures. The measurements have been performed in $n = 5$ independent, non-overlapping, fields (400 x 400 μm) for each dose of glucose and sampling time. In the initial condition (T0), at a confluence value 0.4, each field contained, on average, 150 cells. The HN9.10e cell line (embryonic hippocampal neurons), developed by Lee H.J. et al., was a kind gift of Dr. Kieran C. Breen, Ninewells Hospital & Medical School, Dundee DD1 9SY, UK. For a detailed description of the cell line see the original paper [62].

Results were expressed as mean ± SD, and statistical significance of the differences was assessed by two-way ANOVA for a normal distribution of data. A $p < 0.01$ value was considered as significant

4.3. Experiments to exclude an artifactual origin of CCM exo-metabolites.

To rule out a possible artifactual origin of specific extracellular metabolites in CCM (such as, in particular, ethanol and BA) several control experiments were performed in different conditions. First of all, cell-free CCM was incubated in sealed flasks (N=3) at 37 °C for various times, up to 25 days. Neither ethanol nor BA were detected in this experimental condition, excluding that they may originate from CCM degradation. Furthermore, to obtain a strong evidence that HN9.10e cultures are sterile and free from even the slightest bacterial contamination, we collected 500 μL of CCM from every experimental flask. These aliquots were added to control flasks containing 5 mL of fresh medium and incubated at 37 °C up to 25 days. Over such long times, any minimal bacterial contamination would amplify and become evident. However, neither bacterial growth, nor EtOH and BA were detected in the control flasks, excluding a bacterial origin of these compounds.

4.4. Targeted metabolomics, data processing and statistical analysis.

CCM was analyzed by HPLC-DAD and SPME-HS-GC-MS methods developed and validated in previous works[63,64]. For the analysis, 5 mL of CCM were removed from the flasks and collected in 10 mL headspace vials (Agilent Technologies, Part No. 8010–0038). The vials were sealed with holed screw-caps equipped with Teflon/silicone septa for use with the CombiPAL (Agilent Technologies, Part No. 8010–0139) and kept at -20°C until the analysis. The transfer of such volumes was accomplished using adjustable pipettes and, for better precision, all aliquots were weighted. Details regarding both methods and acquisition parameters are listed in Supplementary Table S5.

For SPME-HS-GC-MS, the chromatographic peak for ethanol was detected and integrated by the GC/MSD ChemStation software (version E.02.02 Agilent Technologies, USA). A calibration curve was built for quantitative purposes analyzing 5 mL of 0, 0.023, 0.046, 0.23, 0.46 and 2.3 mM EtOH (primary standard solution) introduced in 10 mL headspace vials. The mass spectrum of ethanol has been provided in Supplementary Material.

For RP-HPLC-DAD analysis, samples were diluted 5 times in 5 mM sulphuric acid, filtered using a 0.20 μm RC Mini-Uniprep (Agilent Technologies, Italy) and injected in the HPLC system. The identification of metabolites was based on the comparison of the retention time and UV spectra of standard compounds. The 220 nm detection was selected to control the interference of high absorbing compounds, the signals were manually integrated, and the concentration obtained by building a calibration curve with the corresponding analytical standard.

A data matrix was then prepared, having each sample in rows and SPME-HS-GC-MS/HPLC-DAD data of each metabolite in columns, and evaluated by a tailored in-house R-script (R version 3.6.3 (R Development Core Team 2012) and R-Studio, Version 1.1.463). The missing values were replaced with a half of the minimum value found in the data set, and for each glucose concentration-time point pair the average and standard deviation from the analysis of two independent batches were calculated. For all statistical analyses, the concentrations were normalized by cell confluency, transformed by cube root and Pareto scaled. Data normalization to cell number found its admissibility in the work of Muschet and coworkers [65], which found that the concentrations of most metabolites belonging to different classes is positively correlated with the cell number in a linear fashion.

Missing values were replaced by a random value comprised between zero and the detection limit of the corresponding analyte. The R-packages FactoMineR, factoextra, ggpubr, tidyverse and rstatix were used for principal component analysis (PCA) and for data visualization, respectively. 3-way PCA was performed with the open-source Chemometric Agile Tool (CAT) program (http://www.gruppochemiometria.it/index.php/software/19-download-the-r-based-chemometric-software).

For each glucose treatment, cell cultures were growth in duplicate, CCM collected at five different times, and 22 variables quantified by HPLC-DAD and SPME-HS-GC-MS. Thus, the real structure of the datasets can be identified as a parallelepiped whose size was 3 × 22 × 5. In order to apply standard PCA, the three-way data array was matricized to obtain a two-way data table, having 15 rows (3 samples × 5 times) and 22 columns. Before 3-way PCA the cubic data matrix was *j*-scaled to remove the differences among the variables without removing the differences among the objects and among the sampling times.

5. Conclusions

The number of metabolomics studies applied to cell-cultures is still low if reported to the plenty of existing literature on animal models or human body fluids,[66] and the available data in this area are often fragmented. Our study represents a tile in the exploration of cell metabolome, aiming to clarify with a simple targeted approach the unbalances deriving from high-glucose environments in HN9.10e immortalized neurons.

Despite the huge amount of cellular metabolite involved in the response to hyperglycemia, and despite the apparent unaltered neuron morphology and vitality at least up to 120 h, the proposed

experimental design and data processing allowed us the identification of two main metabolites increasing in HN9.10e immortalized cell line treated with 50 and 75 mM glucose with respect to control cultured in 25 mM glucose: NAD^+ and butyric acid.

These two molecules are known to act as signaling molecules and suggest (i) a hyperglycemia-induced switch of neuronal metabolism toward glycolytic pathway as energetic source and toward pentose phosphate pathway as "safety procedure" to increase NADPH production; (ii) an "attempt" of fatty acid synthesis due to the excess of acetyl-CoA. The metabolic alteration is evidenced only by a sudden, massive cell death classified as necrosis after 192 h, which reflects serious mitochondrial damage due to ROS accumulation, in agreement with previous metabolomic studies on the effects of glucose on different cell lines from hippocampus.

Supplementary Materials: The following are available online, Figure S1: Accumulation rate of the quantified metabolites per 24h/normalized confluency expressed as difference between the normalized concentration at each sampling time point and the previous one. Error bars denote standard error of mean (SE), Figure S2: Comparison between the mass spectrum of ethanol detected in CCM (red spectrum) and the NIST reference (blue spectrum), Table S1: Experimental design, Table S2: Concentrations of the quantified metabolites (mean and standard deviation), Table S3: PCA scores, Table S4: PCA loadings, Table S5: HPLC-DAD and HS-SPME-GC-MS experimental conditions.

Author Contributions: All authors contributed toward design of the research, in interpretation of results, and in writing the paper. L.C. performed cell imaging by differential interference contrast microscopy. M.O. prepared the samples and performed SPME-HS-GC-MS analysis, R.N and E.B. performed HPLC-DAD analysis, and B.C performed statistical analysis.

Data Availability Statement: The data presented in this study are available in supplementary material.

Conflicts of Interest: The authors declare no conflict of interest.

References

1. Mergenthaler, P.; Lindauer, U.; Dienel, G.A.; Meisel, A. Sugar for the brain: the role of glucose in physiological and pathological brain function. *Trends Neurosci.* **2013**, *36*, 587–597.
2. Sibson, N.R.; Dhankhar, A.; Mason, G.F.; Rothman, D.L.; Behar, K.L.; Shulman, R.G. Stoichiometric coupling of brain glucose metabolism and glutamatergic neuronal activity. *Proc. Natl. Acad. Sci.* **1998**, *95*, 316 LP – 321, doi:10.1073/pnas.95.1.316.
3. Huang, C.W.; Huang, C.C.; Cheng, J.T.; Tsai, J.J.; Wu, S.N. Glucose and hippocampal neuronal excitability: Role of ATP-sensitive potassium channels. *J. Neurosci. Res.* **2007**, *85*, 1468–1477, doi:10.1002/jnr.21284.
4. Dunn-Meynell, A.A.; Rawson, N.E.; Levin, B.E. Distribution and phenotype of neurons containing the ATP-sensitive K+ channel in rat brain. *Brain Res.* **1998**, *814*, 41–54, doi:https://doi.org/10.1016/S0006-8993(98)00956-1.
5. Cho, S.J.; Kang, K.A.; Piao, M.J.; Ryu, Y.S.; Fernando, P.D.S.M.; Zhen, A.X.; Hyun, Y.J.; Ahn, M.J.; Kang, H.K.; Hyun, J.W. 7,8-dihydroxyflavone protects high glucose-damaged neuronal cells against oxidative stress. *Biomol. Ther.* **2019**, *27*, 85–91, doi:10.4062/biomolther.2018.202.
6. Macauley, S.L.; Stanley, M.; Caesar, E.E.; Yamada, S.A.; Raichle, M.E.; Perez, R.; Mahan, T.E.; Sutphen, C.L.; Holtzman, D.M. Hyperglycemia modulates extracellular amyloid-β concentrations and neuronal activity in vivo. *J. Clin. Invest.* **2015**, *125*, 2463–2467, doi:10.1172/JCI79742.
7. Liu, D.; Zhang, H.; Gu, W.; Zhang, M. Effects of exposure to high glucose on primary cultured hippocampal neurons: involvement of intracellular ROS accumulation. *Neurol. Sci.* **2014**, *35*, 831–837.
8. Russel, J.W.; Golovoy, D.; Vincent, A.M.; Mahendru, P.I.A.; Olzmann, J.A.; Mentzer, A.; Feldman, E. High glucose-induced oxidative stress and mitochondrial dysfunction in neurons. *FASEB J.* **2002**, *16*, 1738–1748.
9. Peng, Y.; Liu, J.; Shi, L.; Tang, Y.; Gao, D.; Long, J.; Liu, J. Mitochondrial dysfunction precedes depression of AMPK/AKT signaling in insulin resistance induced by high glucose in primary cortical neurons. *J. Neurochem.* **2016**, *137*, 701–713.
10. Stranahan, A.M.; Arumugam, T. V; Cutler, R.G.; Lee, K.; Egan, J.M.; Mattson, M.P. Diabetes impairs hippocampal function through glucocorticoid-mediated effects on new and mature neurons. *Nat. Neurosci.* **2008**, *11*, 309–317.
11. Dayer, A.G.; Cleaver, K.M.; Abouantoun, T.; Cameron, H.A. New GABAergic interneurons in the adult neocortex and striatum are generated from different precursors. *J. Cell Biol.* **2005**, *168*, 415–427.
12. Gould, E.; Reeves, A.J.; Graziano, M.S.A.; Gross, C.G. Neurogenesis in the neocortex of adult primates. *Science (80-.).* **1999**, *286*, 548–552.
13. Gonçalves, J.T.; Schafer, S.T.; Gage, F.H. Adult neurogenesis in the hippocampus: from stem cells to behavior. *Cell* **2016**, *167*, 897–914.
14. Deng, W.; Aimone, J.B.; Gage, F.H. New neurons and new memories: how does adult hippocampal neurogenesis affect learning and memory? *Nat. Rev. Neurosci.* **2010**, *11*, 339–350.

15. Kempermann, G.; Kuhn, H.G.; Gage, F.H. More hippocampal neurons in adult mice living in an enriched environment. *Nature* **1997**, *386*, 493–495.
16. Danzer, S.C. Depression, stress, epilepsy and adult neurogenesis. *Exp. Neurol.* **2012**, *233*, 22–32.
17. Apple, D.M.; Fonseca, R.S.; Kokovay, E. The role of adult neurogenesis in psychiatric and cognitive disorders. *Brain Res.* **2017**, *1655*, 270–276.
18. Mule, N.K.; Singh, J.N. Diabetes mellitus to neurodegenerative disorders: is oxidative stress fueling the flame? *CNS Neurol. Disord. Targets (Formerly Curr. Drug Targets-CNS Neurol. Disord.* **2018**, *17*, 644–653.
19. Bartsch, T.; Wulff, P. The hippocampus in aging and disease: From plasticity to vulnerability. *Neuroscience* **2015**, *309*, 1–16, doi:10.1016/j.neuroscience.2015.07.084.
20. Zhao, L.; Dong, M.; Wang, D.; Ren, M.; Zheng, Y.; Zheng, H.; Li, C.; Gao, H. Characteristic metabolic alterations identified in primary neurons under high glucose exposure. *Front. Cell. Neurosci.* **2018**, *12*, doi:10.3389/fncel.2018.00207.
21. Colombaioni, L.; Frago, L.M.; Varela-Nieto, I.; Pesi, R.; Garcia-Gil, M. Serum deprivation increases ceramide levels and induces apoptosis in undifferentiated HN9. 10e cells. *Neurochem. Int.* **2002**, *40*, 327–336.
22. Lee, H.J.; Hammond, D.N.; Large, T.H.; Roback, J.D.; Sim, J.A.; Brown, D.A.; Otten, U.H.; Wainer, B.H. Neuronal properties and trophic activities of immortalized hippocampal cells from embryonic and young adult mice. *J. Neurosci.* **1990**, *10*, 1779–1787.
23. Rello, S.; Stockert, J.C.; Moreno, V.L.; Gamez, A.; Pacheco, M.; Juarranz, A.; Canete, M.; Villanueva, A. Morphological criteria to distinguish cell death induced by apoptotic and necrotic treatments. *Apoptosis* **2005**, *10*, 201–208.
24. Bramanti, E.; Onor, M.; Colombaioni, L. Neurotoxicity Induced by Low Thallium Doses in Living Hippocampal Neurons: Evidence of Early Onset Mitochondrial Dysfunction and Correlation with Ethanol Production. *ACS Chem. Neurosci.* **2018**, *10*, 451–459.
25. Colombaioni, L.; Onor, M.; Benedetti, E.; Bramanti, E. Thallium stimulates ethanol production in immortalized hippocampal neurons. *PLoS One* **2017**, *12*, e0188351.
26. Leardi, R. Chemometrics in data analysis, *Chromatographic Analysis of the Environment* **2006**, 221-241.
27. Wallace, M.; Whelan, H.; Brennan, L. Metabolomic analysis of pancreatic beta cells following exposure to high glucose. *Biochim. Biophys. Acta (BBA)-General Subj.* **2013**, *1830*, 2583–2590.
28. Meissen, J.K.; Hirahatake, K.M.; Adams, S.H.; Fiehn, O. Temporal metabolomic responses of cultured HepG2 liver cells to high fructose and high glucose exposures. *Metabolomics* **2015**, *11*, 707–721.
29. Bernardo-Bermejo, S.; Sánchez-López, E.; Castro-Puyana, M.; Benito-Martínez, S.; Lucio-Cazaña, F.J.; Marina, M.L. A Non-Targeted Capillary Electrophoresis-Mass Spectrometry Strategy to Study Metabolic Differences in an In Vitro Model of High-Glucose Induced Changes in Human Proximal Tubular HK-2 Cells. *Molecules* **2020**, *25*, 512.
30. Bernardo-Bermejo, S.; Sánchez-López, E.; Castro-Puyana, M.; Benito, S.; Lucio-Cazaña, F.J.;

Marina, M.L. An untargeted metabolomic strategy based on liquid chromatography-mass spectrometry to study high glucose-induced changes in HK-2 cells. *J. Chromatogr. A* **2019**, *1596*, 124–133.

31. Wei, P.Z.; Fung, W.W.-S.; Ng, J.K.-C.; Lai, K.-B.; Luk, C.C.-W.; Chow, K.M.; Li, P.K.-T.; Szeto, C.C. Metabolomic changes of Human proximal tubular cell Line in High Glucose environment. *Sci. Rep.* **2019**, *9*, 1–7.

32. Gruetter, R.; Novotny, E.J.; Boulware, S.D.; Rothman, D.L.; Mason, G.F.; Shulman, G.I.; Shulman, R.G.; Tamborlane, W. V Direct measurement of brain glucose concentrations in humans by 13C NMR spectroscopy. *Proc. Natl. Acad. Sci. U. S. A.* **1992**, *89*, 1109–1112, doi:10.1073/pnas.89.3.1109.

33. Huang, Y.; Xiong, Z.-G. Choosing an appropriate glucose concentration according to different cell types and experimental purposes is very important. *Cell Stress Chaperones* **2015**, *20*, 1–2, doi:10.1007/s12192-014-0547-y.

34. Yang, R.-H.; Lin, J.; Hou, X.-H.; Cao, R.; Yu, F.; Liu, H.-Q.; Ji, A.-L.; Xu, X.-N.; Zhang, L.; Wang, F. EFFECT OF DOCOSAHEXAENOIC ACID ON HIPPOCAMPAL NEURONS IN HIGH-GLUCOSE CONDITION: INVOLVEMENT OF PI3K/AKT/NUCLEAR FACTOR-kappa B-MEDIATED INFLAMMATORY PATHWAYS. *Neuroscience* **2014**, *274*, 218–228, doi:10.1016/j.neuroscience.2014.05.042.

35. Wang, H.; Deng, J.; Chen, L.; Ding, K.; Wang, Y. Acute glucose fluctuation induces inflammation and neurons apoptosis in hippocampal tissues of diabetic rats. *J. Cell. Biochem.*, doi:10.1002/jcb.29523.

36. Oliveira, S.R.; Amaral, J.D.; Rodrigues, C.M.P. Mechanism and disease implications of necroptosis and neuronal inflammation. *Cell Death Dis.* **2018**, *9*, 903, doi:10.1038/s41419-018-0872-7.

37. Pierre, K.; Pellerin, L. Monocarboxylate Transporters. *Encycl. Neurosci.* **2009**, 961–965, doi:10.1016/B978-008045046-9.01714-9.

38. Brauburger, K.; Burckhardt, G.; Burckhardt, B.C. The sodium-dependent di- and tricarboxylate transporter, NaCT, is not responsible for the uptake of D-, L-2-hydroxyglutarate and 3-hydroxyglutarate into neurons. *J. Inherit. Metab. Dis.* **2011**, *34*, 477–482, doi:10.1007/s10545-010-9268-2.

39. Antoshechkin, A.G. On intracellular formation of ethanol and its possible role in energy metabolism. *Alcohol Alcohol* 2001, *36*, 608.

40. Allaman, I.; Magistretti, P.J. Chapter 12 - Brain Energy Metabolism. In; Squire, L.R., Berg, D., Bloom, F.E., du Lac, S., Ghosh, A., Spitzer, N.C.B.T.-F.N. (Fourth E., Eds.; Academic Press: San Diego, 2013; pp. 261–284 ISBN 978-0-12-385870-2.

41. Liu, D.; Pitta, M.; Mattson, M.P. Preventing NAD(+) depletion protects neurons against excitotoxicity: bioenergetic effects of mild mitochondrial uncoupling and caloric restriction. *Ann. N. Y. Acad. Sci.* **2008**, *1147*, 275–282, doi:10.1196/annals.1427.028.

42. Aman, Y.; Qiu, Y.; Tao, J.; Fang, E.F. Therapeutic potential of boosting NAD+ in aging and age-related diseases. *Transl. Med. Aging* **2018**, *2*, 30–37, doi:https://doi.org/10.1016/j.tma.2018.08.003.

43. Yoshino, J.; Baur, J.A.; Imai, S. NAD+ Intermediates: The Biology and Therapeutic Potential of NMN and NR. *Cell Metab.* **2018**, *27*, 513–528, doi:https://doi.org/10.1016/j.cmet.2017.11.002.

44. Hou, Y.; Lautrup, S.; Cordonnier, S.; Wang, Y.; Croteau, D.L.; Zavala, E.; Zhang, Y.; Moritoh, K.; O'Connell, J.F.; Baptiste, B.A.; et al. NAD(+) supplementation normalizes key Alzheimer's features and DNA damage responses in a new AD mouse model with introduced DNA repair deficiency. *Proc. Natl. Acad. Sci. U. S. A.* **2018**, *115*, E1876–E1885, doi:10.1073/pnas.1718819115.

45. Katsyuba, E.; Romani, M.; Hofer, D.; Auwerx, J. NAD+ homeostasis in health and disease. *Nat. Metab.* **2020**, *2*, 9–31, doi:10.1038/s42255-019-0161-5.

46. Mori, V.; Amici, A.; Mazzola, F.; Di Stefano, M.; Conforti, L.; Magni, G.; Ruggieri, S.; Raffaelli, N.; Orsomando, G. Metabolic Profiling of Alternative NAD Biosynthetic Routes in Mouse Tissues. *PLoS One* **2014**, *9*, e113939.

47. Liu, D.; Chan, S.L.; de Souza-Pinto, N.C.; Slevin, J.R.; Wersto, R.P.; Zhan, M.; Mustafa, K.; de Cabo, R.; Mattson, M.P. Mitochondrial UCP4 mediates an adaptive shift in energy metabolism and increases the resistance of neurons to metabolic and oxidative stress. *Neuromolecular Med.* **2006**, *8*, 389–414, doi:10.1385/NMM:8:3:389.

48. Bonkowski, M.S.; Sinclair, D.A. Slowing ageing by design: the rise of NAD(+) and sirtuin-activating compounds. *Nat. Rev. Mol. Cell Biol.* **2016**, *17*, 679–690, doi:10.1038/nrm.2016.93.

49. Cueno, M.E.; Kamio, N.; Seki, K.; Kurita-Ochiai, T.; Ochiai, K. High butyric acid amounts induce oxidative stress, alter calcium homeostasis, and cause neurite retraction in nerve growth factor-treated PC12 cells. *Cell Stress Chaperones* **2015**, *20*, 709–713, doi:10.1007/s12192-015-0584-1.

50. Cayo, M.A.; Cayo, A.K.; Jarjour, S.M.; Chen, H. Sodium butyrate activates Notch1 signaling, reduces tumor markers, and induces cell cycle arrest and apoptosis in pheochromocytoma. *Am. J. Transl. Res.* **2009**, *1*, 178–183.

51. Sharma, D.; Singh, J.N.; Sharma, S.S. Effects of 4-phenyl butyric acid on high glucose-induced alterations in dorsal root ganglion neurons. *Neurosci. Lett.* **2016**, *635*, 83–89, doi:10.1016/j.neulet.2016.10.038.

52. Kim, S.W.; Hooker, J.M.; Otto, N.; Win, K.; Muench, L.; Shea, C.; Carter, P.; King, P.; Reid, A.E.; Volkow, N.D.; et al. Whole-body pharmacokinetics of HDAC inhibitor drugs, butyric acid, valproic acid and 4-phenylbutyric acid measured with carbon-11 labeled analogs by PET. *Nucl. Med. Biol.* **2013**, *40*, 912–918, doi:10.1016/j.nucmedbio.2013.06.007.

53. Shah, P.; Nankova, B.B.; Parab, S.; La Gamma, E.F. Short chain fatty acids induce TH gene expression via ERK-dependent phosphorylation of CREB protein. *Brain Res.* **2006**, *1107*, 13–23, doi:https://doi.org/10.1016/j.brainres.2006.05.097.

54. Nankova, B.B.; Agarwal, R.; MacFabe, D.F.; La Gamma, E.F. Enteric Bacterial Metabolites Propionic and Butyric Acid Modulate Gene Expression, Including CREB-Dependent Catecholaminergic Neurotransmission, in PC12 Cells - Possible Relevance to Autism Spectrum Disorders. *PLoS One* **2014**, *9*, e103740.

55. Freeman, W.H.; Learning, S. *Principles of Biochemistry*; Nelson, D.L., Cox, M.M., Eds.; Seventh.; macmillan learning, 2017;

56. Herrero-Mendez, A.; Almeida, A.; Fernández, E.; Maestre, C.; Moncada, S.; Bolaños, J.P. The

bioenergetic and antioxidant status of neurons is controlled by continuous degradation of a key glycolytic enzyme by APC/C–Cdh1. *Nat. Cell Biol.* **2009**, *11*, 747–752, doi:10.1038/ncb1881.

57. Bolaños, J.P.; Almeida, A.; Moncada, S. Glycolysis: a bioenergetic or a survival pathway? *Trends Biochem. Sci.* **2010**, *35*, 145–149, doi:https://doi.org/10.1016/j.tibs.2009.10.006.

58. Nochi, Z.; Olsen, R.K.J.; Gregersen, N. Short-chain acyl-CoA dehydrogenase deficiency: from gene to cell pathology and possible disease mechanisms. *J. Inherit. Metab. Dis.* **2017**, *40*, 641–655, doi:10.1007/s10545-017-0047-1.

59. Chen, J.S.; Faller, D. V; Spanjaard, R.A. Short-chain fatty acid inhibitors of histone deacetylases: promising anticancer therapeutics? *Curr. Cancer Drug Targets* **2003**, *3*, 219–236, doi:10.2174/1568009033481994.

60. Graber, R.; Sumida, C.; Nunez, E.A. Fatty acids and cell signal transduction. *J. Lipid Mediat. Cell Signal.* **1994**, *9*, 91–116.

61. Gray, M.W.; Burger, G.; Lang, B.F. Mitochondrial evolution. *Science (80-.).* **1999**, *283*, 1476–1481.

62. Lee, H.J.; Hammond, D.N.; Large, T.H.; Roback, J.D.; Sim, J.A.; Brown D.A.; Otten U.H.; Wainer B.H. Neuronal properties and trophic activities of immortalized hippocampal cells from embryonic and young adult mice. *J. Neurosci.* **1990**. *10*, 1779-1787, doi:10.1523/JNEUROSCI.10-06-01779.1990

63. Campanella, B.; Onor, M.; Lomonaco, T.; Benedetti, E.; Bramanti, E. HS-SPME-GC-MS approach for the analysis of volatile salivary metabolites and application in a case study for the indirect assessment of gut microbiota. *Anal. Bioanal. Chem.* **2019**, *411*, 7551–7562, doi:10.1007/s00216-019-02158-6.

64. Campanella, B.; Lomonaco, T.; Benedetti, E.; Onor, M.; Nieri, R.; Bramanti, E. Validation and Application of a Derivatization-Free RP-HPLC-DAD Method for the Determination of Low Molecular Weight Salivary Metabolites. *Int. J. Environ. Res. Public Heal.* **2020**, *17*, 6158.

65. Muschet, C.; Möller, G.; Prehn, C.; de Angelis, M.H.; Adamski, J.; Tokarz, J. Removing the bottlenecks of cell culture metabolomics: fast normalization procedure, correlation of metabolites to cell number, and impact of the cell harvesting method. *Metabolomics* **2016**, *12*, 151.

66. León, Z.; García-Cañaveras, J.C.; Donato, M.T.; Lahoz, A. Mammalian cell metabolomics: experimental design and sample preparation. *Electrophoresis* **2013**, *34*, 2762–2775.